# The $^{12}C(\gamma,NN)$ reaction studied over a wide kinematic range

D. P. Watts,[1] I. J. D. MacGregor,[1] J. Ahrens,[4] J. R. M. Annand,[1] R. Beck,[4] D. Branford,[2] P. Grabmayr,[3] S. J. Hall,[1] P. D. Harty,[1,*] T. Hehl,[3] J. D. Kellie,[1] T. Lamparter,[3] M. Liang,[2,†] J. A. MacKenzie,[2,‡] S. J. McAllister,[1,§] J. C. McGeorge,[1] R. O. Owens,[1] M. Sauer,[3] R. Schneider,[3] G. J. Wagner,[3] and T. T-H. Yau[1,‖]

[1]*Department of Physics and Astronomy, University of Glasgow, Glasgow G12 8QQ, United Kingdom*

[2]*Department of Physics and Astronomy, University of Edinburgh, Edinburgh EH9 3JZ, United Kingdom*

[3]*Physikalisches Institut, Universität Tübingen, D-72076 Tübingen, Germany*

[4]*Institut für Kernphysik, Universität Mainz, D-55099 Mainz, Germany*

(Received 23 November 1999; published 21 June 2000)

The $^{12}C(\gamma,np)$ and $^{12}C(\gamma,pp)$ reactions have been studied using the Glasgow photon tagging spectrometer at the Mainz MAMI electron microtron for $E_\gamma = 150-700$ MeV over a kinematic range which extends well beyond the approximately back-to-back detector arrangements of previous work. For $^{12}C(\gamma,np)$ the general trends of the missing energy distributions are reproduced over a wide range of kinematics and photon energies by the theory developed by the Valencia group. The corresponding $^{12}C(\gamma,pp)$ channel is overestimated by a factor of $\sim 3$. Detailed comparisons of the experimental data with a Monte Carlo simulation of the direct $2N$ knockout process provide the first evidence above the $\Delta$ resonance for direct $2N$ knockout and show that this process dominates the $^{12}C(\gamma,np)$ reaction at low missing energies up to $E_\gamma \sim 700$ MeV. The $^{12}C(\gamma,pp)$ reaction is somewhat less well described by the Monte Carlo simulation. A possible explanation of the observed discrepancies within a direct $2N$ framework is presented. At high recoil momenta both $2N$ reaction channels exhibit an excess yield compared to the Monte Carlo prediction of direct $2N$ knockout. The excess yield in this region is compared with the predicted effects of short-range correlations and with the predicted contributions due to other reaction mechanisms.

PACS number(s): 25.20.Lj, 27.20.+n

## I. INTRODUCTION

The study of the photoemission of nucleon pairs from the nucleus was originally thought to be a good tool for studying short-range correlations. It was later realized that several mechanisms will play a role in these reactions and may make it difficult to extract information on correlations. Our understanding of the different processes involved has only progressed significantly in quite recent years, through major improvements in both the quality of the experimental data and in the theoretical description of the photoemission process.

When a photon is absorbed by a nucleus the different absorption processes and final-state interactions (FSI's) pose a complicated theoretical problem. In particular FSI's produce two-step reaction processes which make information about the initial state difficult to extract. For few-body nuclei the cross sections can be calculated [1] from the basic Feynman diagrams. For heavier nuclei the complexity of the problem renders this approach intractable. The study of heavier nuclei is, however, important, not only to examine contributions from nucleons above the *s* shell, but also to learn more about how the nuclear medium affects the basic processes. In particular, extracting information on modifications to the fundamental *NN* interaction and the role of $\Delta$-*N* and $3N$ interactions require measurements over a wide range of kinematics and photon energy for several nuclei together with a reliable theoretical treatment.

In recent years the Valencia group have developed a microscopic model of photonuclear reactions in heavier nuclei [2]. This includes all the important reaction processes occurring in photon absorption at intermediate energies. The products of these reactions are then tracked through the nuclear medium, using a semiclassical approach to account for any further interactions in the nucleus. The basic absorption processes comprise absorption on two or three nucleons ($2N$/$3N$) and pion production processes ($N\pi$ and $NN\pi$). The pion production processes include both resonant ($\Delta$) and nonresonant terms and include the propagation and interaction of the $\Delta$ in the medium. The model accounts for both long- and short-range correlation effects, with the latter included by the use of correlated nucleon pair wave functions which are consistent with the expected *NN* repulsion at short range. Nucleons produced from the initial reaction processes can be scattered by the medium, while pions can be scattered or reabsorbed in $(\pi,NN)$ and $(\pi,NNN)$ reactions. The model has been shown to give a good account of all of these processes in a comparison of recent $(\gamma,np)$ data presented as a function of missing energy, $E_m$ [3,4]. Reference [5] also shows agreement with $(\gamma,np)$ data presented as a function of proton energy, although some proton angle-dependent discrepancies were evident. For the weaker $(\gamma,pp)$ channel the magnitude is overestimated by a factor of $\sim 3$ [3–6] but the general agreement with the shape of the distribution indicates the relative contributions of the different reaction processes are fairly well described.

Although the Valencia model represents a major theoret-

*Present address: School of Physics, University of Melbourne, Australia.

†Present address: Thomas Jefferson Lab, Newport News, VA.

‡Present address: Amadeus Data Processing, Munich, Germany.

§Present address: J.P. Morgan Ltd., London, UK.

‖Present address: Chase Research, Basingstoke, UK.

 

ical advance, allowing the treatment of the full complexity of the photonuclear reaction mechanism, this is achieved at significant cost. The model is based on a nuclear matter approach which, although related to real nuclei by a local-density approximation, neglects binding effects, and ignores nuclear shell structure. Many other theoretical approaches to $(\gamma,NN)$ reactions concentrate exclusively on the direct two nucleon knockout process $(2N)$ leaving the residual nucleus in a low lying, bound state and this more limited aim allows the models to be based on a more realistic description of nuclear structure.

The early theoretical approach of Gottfried [7], which has been the basis of many subsequent experimental analyses, uses a ''zero-range approximation'' for the interaction and restricts the photoabsorption to be on pairs in $S$ relative angular momentum states $(l=0)$ with the additional assumption of outgoing plane waves. The cross section can then be written as the product of $F(P)$, the probability of finding a pair in the nucleus at zero separation with a combined momentum of $P$, and a second term $S_{fi}$ which depends principally on the wave function for the relative motion of the pair. The $F(P)$ distribution is obtained simply from folding two individual nucleon momentum distributions. Due to parity conservation the relative $S$ state is only allowed if the orbital angular momentum due to the motion of the center-of-mass (c.m.) of the pair, $L$, equals 0 or 2 for two $(1p)$ shell nucleons and these two possibilities make up the $(1p)^2$ $F(P)$ distribution. For $(1s1p)$ knockout the parity of the pair is reversed and the $(1s1p)$ $F(P)$ includes only $L=1$. Although correlations between the two knocked out nucleons do not affect their combined momentum distribution, recent calculations [8] using a leading-order approximation have indicated that at large $P$, this distribution is sensitive to short-range correlations with the other (A-2) nucleons. The probability of such large $P$ is small so this does not imply a significant modification of the Gottfried approach. However it does suggest an interesting way to access correlation effects in $2N$ knockout measurements.

In recent years far more detailed microscopic models of $2N$ knockout have become available [9–13]. These models include a distorted wave treatment of the emitted nucleons and a detailed description of the contributing photoabsorption mechanisms, meson exchange currents (MEC's), $\Delta$ contributions and short-range correlations (SRC's) and are leading to a much deeper understanding of $2N$ knockout. In these models the formal factorization, $F(P)\times S_{fi}$, of the Gottfried treatment is lost, although the pair momentum distribution is still a determining factor in the angular correlation of the outgoing nucleons. For the $(\gamma,np)$ reaction above 200 MeV photon energy Refs. [11,13] indicate that absorption on pairs in relative $S$ states is still dominant as assumed in the Gottfried treatment. However, for $(\gamma,pp)$ this simplification has serious shortcomings since some $2N$ knockout mechanisms would be expected to proceed via absorption on pairs in higher relative states of angular momentum. For $(\gamma,np)$ the dominant reaction mechanisms are predicted to be meson and $\Delta$ currents with smaller contributions from mechanisms involving SRC's, although these significantly increase with $E_\gamma$ [10]. Valuable information on the medium range behavior of nucleon pairs in the nuclear medium can be obtained from the two-body mechanisms, which are dominant in this channel at lower photon energies. The $(\gamma,pp)$ reaction is expected to be more sensitive to SRC's due to the suppression of charged MEC's, although recent calculations predict $\Delta$ mechanisms dominate the cross section for $E_\gamma \leqslant 300$ MeV [10,13]. Above the $\Delta$ resonance the relative role of SRC's is predicted to increase considerably with a third of the $(\gamma,pp)$ cross section at $E_\gamma=400$ MeV attributable to SRC mechanisms [14]. The maximum sensitivity to SRC's is predicted to occur for photoabsorption on pairs in relative $^1S_0$ states as the proton-proton pair is at close range and the contribution of the dominant $M1$ component for $2N$ knockout involving intermediate $\Delta$ excitation $(\Delta N \rightarrow NN)$ is suppressed [15].

Many recent photonuclear experiments above 100 MeV have concentrated on $2N$ emission [3–6,16–23]. Measurements of the recoil momentum distributions in the $^{12}\mathrm{C}(\gamma,np)$ and $^{12}\mathrm{C}(\gamma,pp)$ reactions have been obtained over a wide photon energy range $(E_\gamma=150$–$400$ MeV) and with good energy resolution in the so-called quasideuteron (QD) kinematics, detecting outgoing nucleons near to the back-to-back angular correlation which results from photon absorption on stationary initial pairs [16,21]. A Monte Carlo (MC) model of the direct $2N$ knockout process, which simulates the measured pair momentum distribution on the basis of the Gottfried model assumptions gave a good description of the shape of the $(\gamma,np)$ momentum distribution and only slightly poorer agreement for $(\gamma,pp)$ in the missing energy, $E_m$, regions corresponding to absorption on $(1p)^2$ pairs. The $(\gamma,np)$ data for the higher $E_m$ region, which is populated by absorption on $(1s1p)$ pairs, was also found to be quite well described by the MC model. These results suggest that the $2N$ mechanism is dominant at low $E_m$. However the near-QD kinematics employed strongly biases the detection efficiency in favor of the direct $2N$ knockout mechanism so that measurements over a wider kinematic range could still show a significant contribution from other mechanisms to the overall $(\gamma,NN)$ yield.

Subsequent measurements of the angular distributions of back-to-back pairs from the $(1p)^2$ shells of $^{12}$C [23] showed large differences between $(\gamma,np)$ and $(\gamma,pp)$ indicating different microscopic mechanisms for the two reactions. The dissimilar shapes also gave a strong indication that final-state interactions (FSI's) following an initial $(\gamma,np)$ reaction do not dominate the $(\gamma,pp)$ yield for this low $E_m$ region. Predictions from the microscopic code of Ryckebusch [12] reproduce the general features of the angular distributions and give a good description of the energy dependence of both reactions.

Recent measurements with polarized photons have illustrated the limitations of the Gottfried assumptions. Measurements of the asymmetry for the $^{12}C(\vec{\gamma},pp)$ reaction at Mainz [24] and a measurement on $^{16}$O at LEGS [25] indicate that the reaction cannot be explained simply by photoabsorption on $pp$ pairs in relative $S$ states. The measured asymmetries for the $(\vec{\gamma},np)$ reaction on $^{12}$C [26] and $^{16}$O [25] indicate

differences between the $pp$ and $np$ channels at low missing energy.

The present experiment was designed to measure the $(\gamma,NN)$ cross section over a phase space region predominantly away from the usual back-to-back kinematics of previous measurements. This provides a far more stringent test of the photoreaction models, because the relative contributions from different processes are expected to vary considerably over such a region. The wide detector acceptance also allows the $2N$ knockout component of the yield to be studied in kinematic regions where the initial momentum of the nucleon pair is necessarily large. This range of pair momenta and the similarly wide photon energy range of the present data will test the limitations of the previous analyses [16–21], in which it was assumed that the variation of the $(\gamma,NN)$ cross section is dominated by its proportionality to $F(P)$, which was calculated using harmonic oscillator wave functions and the Gottfried prescription. The pair momenta also reach the region in which sensitivity to SRC's is predicted [8]. In addition, the cross section in regions where $2N$ knockout is not dominant allows a more quantitative assessment of the possible contribution of other processes at low $E_m$, information which is particularly important for comparison of data with modern microscopic models.

## II. EXPERIMENT

The experiment was carried out at the 855 MeV Mainz microtron (MAMI-B) [27] using the Glasgow tagged-photon spectrometer [28] together with two plastic scintillator arrays to detect the emitted nucleons. The photon beam was collimated 2.5 m downstream from the radiator by a circular 5 mm diameter aperture. This produced a resultant beam spot diameter of $\sim$1.5 cm at the target. The tagging efficiency (fraction of tagged photons reaching the target) was measured in separate experimental runs at reduced beam intensity with a lead glass detector placed in the photon beam line. The average value was found to be $\sim$56%. During normal runs the photon beam intensity and position were monitored using an ion chamber and high sensitivity TV camera placed downstream of the target.

The positioning of the detectors for the experiment is shown in Fig. 1. Protons were detected in a charged particle hodoscope (PiP) [29] placed in a backward position covering the polar angular range 78°–158°. The reaction timing was obtained from a segmented half ring of 1 mm thick scintillators ($\Delta E_{\mathrm{PiP}}$) centered on the target and positioned on the PiP side of the photon beam at a radius of $\sim$11 cm. The first level trigger required a hit in PiP along with a hit in a $\Delta E_{\mathrm{PiP}}$ element between PiP and the target.

Coincident protons and neutrons were detected in an array of time-of-flight plastic scintillators (TOF) [30], which were positioned to cover a wide angular range (36.7°–142.0°) opposite PiP and 16°–31° on the PiP side of the beam. The TOF flight paths were in the range 4.0–6.2 m, giving a total solid angle $\Delta\Omega = 0.91$ sr. Separation of charged and uncharged particles in the TOF array was carried out using information from two segmented half rings of scintillator ($\Delta E1$, $\Delta E2$), each 2 mm thick, centered on the target at

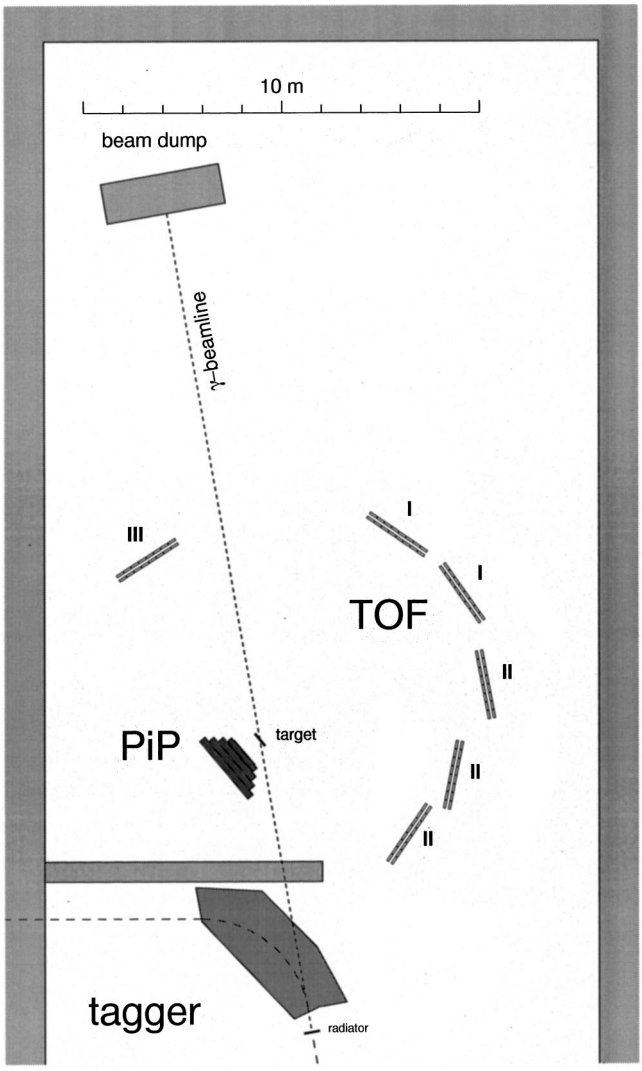


FIG. 1. Layout of the tagger and particle detectors.

radii of $\sim$11 cm and $\sim$30 cm. Compared with previous measurements [3–5,16–23] the addition of the second half ring improves the identification of particles detected in the TOF array. The graphite target, of density 685.3 mg/cm$^2$, was placed at an angle of 45° to the photon beam direction. The background of events not originating from reactions in the target was measured in runs with the target removed. Detector calibrations were carried out using a 216.0 mg/cm$^2$ perdeuterated polyethylene target ($CD_2$). The combined missing energy resolution, averaged over the photon energy range of the experiment, was found to be $\sim$8 MeV [full width at half maximum (FWHM)].

## III. DATA ANALYSIS

The identification of protons in the PiP detector used a range method, the details of which have been described previously [29]. The loss of proton yield through nuclear reactions in the scintillator was corrected by applying an energy dependent weight to the retained proton events, which was calculated from a GEANT [31] simulation of the detector

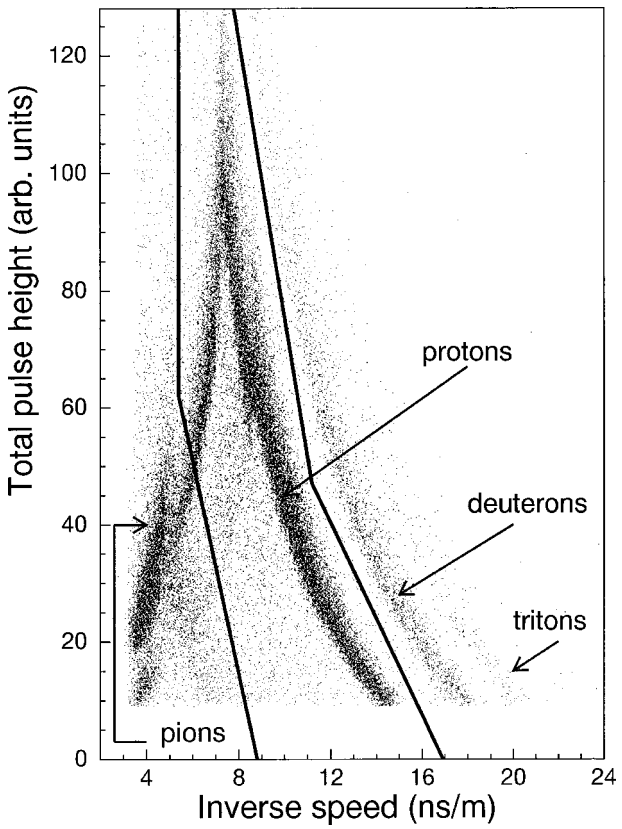


FIG. 2. A 2D plot of pulse height versus inverse speed for charged particles in TOF. The lines on the figure indicate the cut applied to the data to select protons.

[32]. The energy range of the PiP detector was ~31–270 MeV. The minimum energy threshold was determined by the proton energy losses between the reaction vertex and the front face of PiP and the 8 MeV pulse height threshold of PiP. High-energy protons which entered the back layer of PiP were vetoed and a software cut was applied to the remaining proton events to give a well determined maximum energy.

In TOF charged and uncharged particles were distinguished by noting whether the correct $\Delta E1$ and $\Delta E2$ elements fire along the particles' path from the target. To determine the correct $\Delta E$ elements for each TOF bar the pattern of hits in $\Delta E$ elements was examined for single TOF proton events. The TOF detectors were placed two deep to increase the efficiency for the detection of neutrons. For uncharged particles a hit in both front and back layers was assumed to arise from scattering into the back layer. For high-energy charged particles, which could pass through the front TOF layer and into the back layer, the two signals were added to obtain the total TOF pulse height. A plot of total TOF pulse height versus inverse speed for charged particles is shown in Fig. 2. The cut indicated on the figure shows how protons were selected for analysis. For uncharged TOF hits a minimum time-of-flight requirement was imposed to remove the ''$\gamma$ flash'' peak [30].

A pulse height threshold of 9 MeV (electron equivalent) was applied to the TOF detectors to reduce the effect of randoms and to allow a standard threshold to be used for the neutron detection efficiency calculations with the STANTON [33] code. Each neutron event was weighted using the calculated (energy-dependent) efficiency. This ranged from ~11% for 50 MeV neutrons to ~8% at 400 MeV. To remove the region of very low neutron detection efficiency, a software threshold was applied to the speed of the neutrons, equivalent to an energy of 19 MeV. The maximum neutron energy (~640 MeV) was determined by the software cut required to remove the $\gamma$ flash events. The threshold energy for TOF proton events was determined by the software pulse height threshold of 9 MeV (electron equivalent) at the TOF bar which corresponds to ~35 MeV at the target. The maximum energy of protons detected by TOF was ~190 MeV, determined by the position of the proton-pion separation cut (Fig. 2).

The effect of random coincidences in the tagger and the TOF neutron events were accounted for by using a weight method [34]. Random protons in TOF were found to be negligible due to the additional requirement of a TOF $\Delta E$ hit. Events from prompt time regions were incremented in the final yield with a weight factor of 1. Samples of events outside these regions were identified as random and incremented in the final yield with an appropriate negative weight, scaled to account for the difference in width between the prompt and random regions. The ratio of real to random events in the prompt tagger region was ~3. For TOF neutrons the real to random ratio depended on the neutron angle and varied from ~2 to ~7.

The sources of systematic error in the measured cross sections are discussed in Ref. [4] and are estimated to be up to ±12% for the $(\gamma,np)$ reaction and up to ±11% for the $(\gamma,pp)$ reaction. An overall check of the reliability of the measured cross sections was provided by a measurement of the $D(\gamma,np)$ cross section as a function of $E_\gamma$ using a $CD_2$ target. This was found to agree with previous measurements [35,36] taking account of the statistical (~15%) and systematic (~12%) uncertainty.

An attempt was also made to compare the present data with previous results obtained with the PiP-TOF setup. Since the visible cross sections depend markedly on the detector arrangements, which were different in the earlier work, this comparison has only been possible for a small number of overlapping angles from one previous experiment [23]. The present results are slightly lower than the cross sections reported at low missing energy in Ref. [23] but the difference lies easily within the combined systematic errors.

## IV. REACTION MECHANISMS LEADING TO TWO NUCLEON EMISSION

The results of the present experiment are presented in this and the following section. This section starts by surveying the available data and then discusses what can be learnt about the mechanisms contributing to the photoemission of nucleon pairs by comparing the data with the Valencia model. The following section considers the direct $2N$ knockout mechanism in more detail.

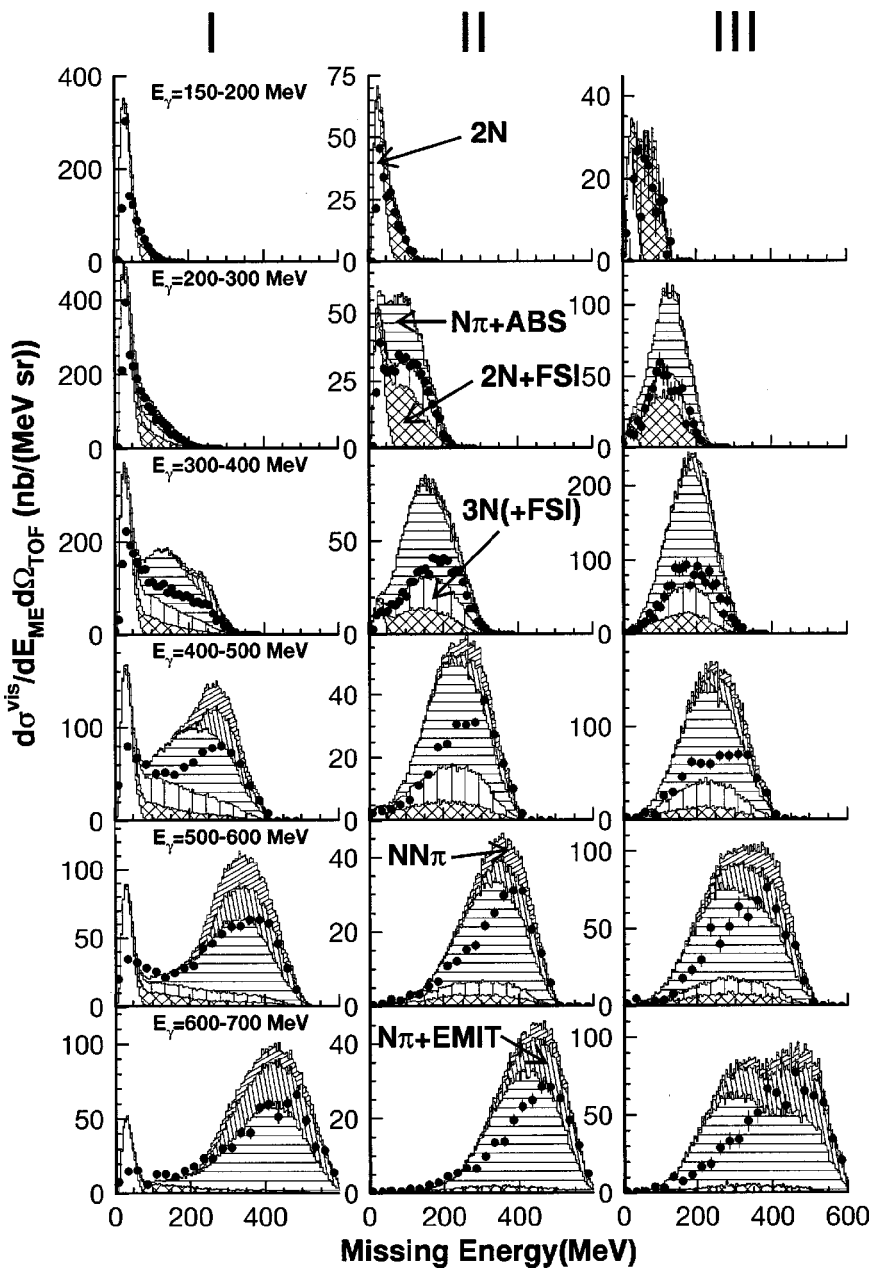


FIG. 3. Missing energy spectra for the $^{12}C(\gamma,np)$ reaction, for the kinematic regions **I**, **II**, and **III** specified in the text. The Valencia model predictions are separated into the direct $2N$ knockout ($2N$), direct $2N$ knockout with FSI ($2N+$FSI), direct $3N$ knockout with or without FSI [$3N(+$FSI)], initial $\pi$ production with subsequent $\pi$ reabsorption in the nucleus ($N\pi+$ABS), initial $\pi$ production followed by $\pi$ rescattering in the nucleus ($N\pi+$EMIT) and initial $NN\pi$ reactions, as indicated in the figure.

### A. General points

The experimental results in Figs. 3–10 are presented in the form of measured visible cross sections ($\sigma^{vis}$) defined simply as the cross section which produces an event within the acceptance of the PiP/TOF detectors. Comparison with theoretical models can be made by filtering the results of the theoretical calculation through a simulation of the detector setup, including the angular and energy acceptances of each detector. The experimental data obtained for the ($\gamma,NN$) reactions are separated into three kinematic regions according to the polar angle of the TOF particle (indicated on Fig. 1). Region **I** was chosen to include back-to-back QD kinematics and covered a polar angle range of 36.7°–71.2°. The other regions sampled progressively more extreme kinematics with polar angle ranges of 78.8°–142.4° for region **II** and 13.7°–30.2° (on the opposite side of the photon beam to the other TOF detectors) for region **III**.

In presenting the ($\gamma,NN$) data two variables, the recoil momentum, $\mathbf{P}_r$, and the missing energy, $E_m$, are of general utility. The momentum of the recoiling system, $\mathbf{P}_r=\mathbf{P}_\gamma-\mathbf{P}_{N1}-\mathbf{P}_{N2}$, is obtained from the measured momenta of the incident photon and the emitted nucleons. If FSI and the effect of the nuclear potential on the outgoing nucleon momenta are neglected, then for absorption by two nucleons the initial pair momentum, $\mathbf{P}$ is given by $\mathbf{P}+\mathbf{P}_r=0$. The $\mathbf{P}$ distributions can be calculated and comparison with the measured $\mathbf{P_r}$ distributions allows the possibility of distinguishing between different absorption mechanisms and also of identifying the presence of more complex mechanisms which involve FSI since this tends to produce higher values of $\mathbf{P}_r$. The missing energy is defined as $E_m=E_\gamma-T_{N1}-T_{N2}-T_r$ where $E_\gamma$ is the incident photon energy, $T_{N1}$ and $T_{N2}$ are the energies of the outgoing nucleons and $T_r$ is the (typically small) energy of the recoiling (A-2) system which is calcu-

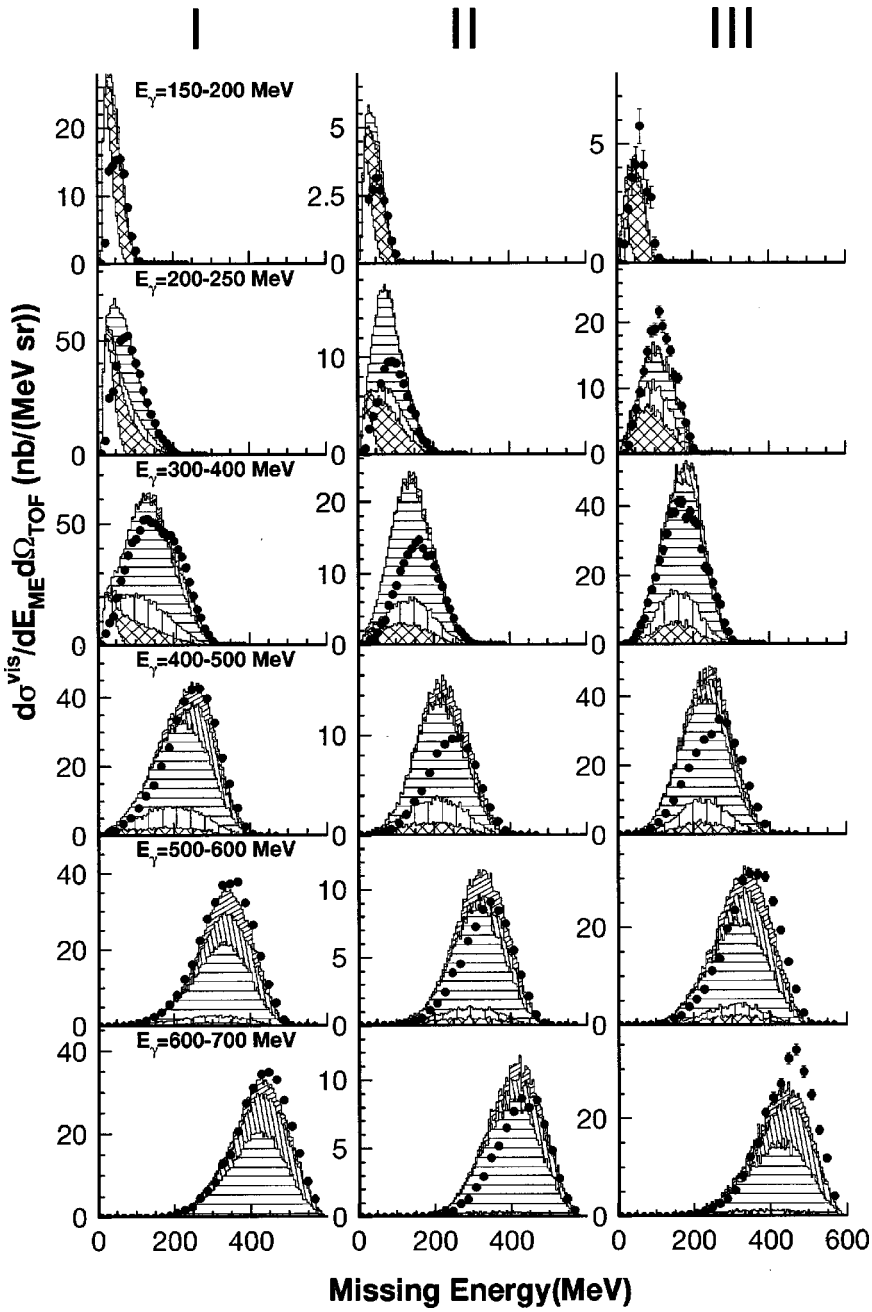


FIG. 4. Missing energy spectra for the $^{12}C(\gamma,pp)$ reaction, for the kinematic regions specified in the text. The Valencia model calculations are distinguished as in Fig. 3 and have been multiplied by a factor of 0.4.

lated from its momentum $\mathbf{P}_r$. The missing energy gives information about the energy associated with excitation of the residual (A-2) system or by other undetected particles and is therefore expected to show sensitivity to the underlying mechanism involved.

### B. The $^{12}C(\gamma,np)$ missing energy spectra

The $E_m$ spectra from the $(\gamma,np)$ measurement in the three kinematic regions are shown in Fig. 3, for photon energy bins up to 700 MeV. The data from region **I** show the characteristic peak at low missing energy corresponding to the residual nucleus being left in or near its ground state. This is generally attributed to the detection of two nucleons ejected by a direct $2N$ knockout process. The strength at low $E_m$ becomes relatively much less important as $E_\gamma$ increases with other processes giving large amounts of strength in regions of higher $E_m$. However significant low $E_m$ strength can be seen up to $E_\gamma=700$ MeV, even though the upper energy cutoff of the detectors reduces the detection probability for low $E_m$ events at high photon energy.

The cross sections for the more backward neutron angles of region **II** show significantly different behavior. For all except the lowest $E_m$ region the cross section decreases relative to region **I** by a roughly $E_\gamma$ independent factor of $\sim 2$. However the low $E_m$ peak decreases by a factor of $\sim 6$ even for the lowest $E_\gamma$ range and by a factor of $\sim 10$ for $E_\gamma=200-300$ MeV. The even more extreme kinematics of region **III**, where both particles are detected on the same side of the beam, produces an even greater depression of the low $E_m$ events and the cross section in this $E_m$ region becomes

extremely small above $E_\gamma = 300$ MeV. The low $E_m$ cross sections in regions **II**, **III** are significantly smaller than in the back-to-back kinematics as the $2N$ knockout processes now require very large initial pair momenta, which have a very small probability in the momentum distribution. For higher $E_m$ events the cross sections are largest at the more forward angles sampled in regions **I** and **III**.

A comparison of the $(\gamma,np)$ missing energy distributions with the predictions of the Valencia model (VM) described in Ref. [2] is shown in Fig. 3. The model treats photon absorption by two nucleons, by three nucleons and also quasifree pion production on a single nucleon, and allows for subsequent scattering of pions and nucleons and for pion reabsorption. Several combinations of these processes are identified in the figure and in the figure caption. It can be seen that $2N$ knockout may be separated reasonably well on the basis of missing energy alone, but the remaining mechanisms cannot be distinguished this way due to their considerable overlap. Undoubtedly better separation could be achieved from the study of energy and angle correlations of the two nucleons, but this has not yet been attempted.

The VM predictions can be seen to describe the general trends of the $(\gamma,np)$ missing energy spectra for all the measured photon energies and kinematics. This gives better confidence in the treatment of the contributing processes by the VM than previous comparisons in more restricted kinematics. Looking in more detail, the VM predictions for region **I** attribute the low $E_m$ peak very largely to $2N$ knockout. The VM gives better agreement in the $2N$ knockout region than is apparent from Fig. 3 as the VM does not include the experimental resolution which deteriorates at higher $E_\gamma$. Comparison of the VM predictions with data integrated over the $2N$ region (Figs. 5 and 6) show quite good agreement in all photon energy regions using a common normalization. At high $E_\gamma$ the $2N$ knockout strength is particularly interesting as the photon must necessarily sample the $NN$ interaction at short range. The VM treatment includes the effects of both $\rho$ meson currents and SRC and if their contributions to the cross section at high $E_\gamma$ turn out to be large, it should be possible to obtain information on these mechanisms from a comparison with the data. This possibility is being investigated.

The large strength at higher $E_m$ ($\geqslant 100$ MeV) in region **I**, which is seen for photon energies $E_\gamma \geqslant 300$ MeV is predicted by the VM to arise mainly from quasifree pion production followed by pion reabsorption (ABS). The model clearly overestimates the strength of this process in the region **I** kinematics although the $E_m$ distribution shape is quite well described. In total the overestimation may be more serious than shown in Fig. 3 since the VM does not include $2\pi$ photoproduction, which is expected to be significant. $2\pi$ photoproduction on the proton is negligible at $E_\gamma \sim 500$ MeV but rises to $\sim 50\%$ of the single $\pi$ production cross section at 700 MeV [37]. A recent theoretical study [38] has indicated that the cross section for $2\pi$ photoproduction may be enhanced in the nucleus compared to the free nucleon due to significant medium modifications of the production process. Also the VM only accounts for the $\Delta$ and does not include the higher excited states of the nucleon which may contribute to the cross section at high $E_\gamma$.

The VM predictions for region **II** again indicate that $2N$ knockout will be dominant at low $E_m$, although with a lower cross section and decreasing with photon energy at a faster rate than region **I**, in agreement with the data, because larger values of the initial pair momentum are involved. The higher $E_m$ regions are predicted to have relative contributions of the different processes similar to region **I**, although FSI following $2N$ and $3N$ absorption has increased. The main FSI strength generally occurs at higher $E_m$ than in region **I** indicating that a lot of the strength comes from harder final-state interaction processes which give more energy to the residual system and spread the strength over a wider $E_m$ range. The dominance of the $N\pi+$ABS process is again evident for $E_\gamma \geqslant 300$ MeV and the overestimation of the data is similar to that observed for region **I**.

Even in the extreme kinematics of region **III** the VM predicts significant $2N$ knockout at low $E_m$ for $E_\gamma$ below 300 MeV and describes the photon energy dependence of its magnitude fairly well. For photon energies through the $\Delta$ resonance the $N\pi+$ABS process is again predicted to give the main contribution and the VM gives a good account of the shape of the missing energy distribution but is less good at predicting the strength.

Although describing the trends of the measured cross sections the VM does not give the same level of agreement observed in comparisons with previous experimental data on $^{12}C(\gamma,pn)$ [3,4] where protons were detected at more forward angles ($51°-129°$) than in this work. A similar angle-dependent discrepancy is indicated in Ref. [5] where the VM gives a good description of the $^{12}C(\gamma,p)$ and $^{12}C(\gamma,np)$ cross sections at forward emission angles for the proton but overestimates the data by a factor of up to $\sim 2$ at more backward emission angles.

### C. The $^{12}C(\gamma,pp)$ missing energy spectra

The measured cross sections for the weaker $(\gamma,pp)$ reaction (Fig. 4) exhibit some different characteristics to those observed for $(\gamma,np)$. A comparison of the low $E_m$ yields shows the $(\gamma,pp)$ cross section is an order of magnitude smaller, due primarily to the suppression of $\Delta$ and charged MEC contributions to the knockout of $pp$ pairs. The low $E_m$ cross section diminishes rapidly with increasing $E_\gamma$ and essentially disappears for $E_\gamma$ above 500 MeV. Some of the reduction in low $E_m$ strength at high photon energies has the same cause as in the $(\gamma,np)$ case, namely the upper limit on the energy acceptance of the particle detectors which is more restrictive for protons than for neutrons. The strength and missing energy variation of the $(\gamma,pp)$ cross section for $E_m \geqslant 100$ MeV varies with $E_\gamma$ and between the three kinematic regions in a very similar way to the $(\gamma,np)$ cross section.

A comparison of the VM model predictions with the $(\gamma,pp)$ missing energy distributions is shown in Fig. 4. The relative contribution of the different processes for $E_m \geqslant 100$ MeV looks similar to $(\gamma,np)$. As has been noted before [3–6] the model overestimates the strength of the $(\gamma,pp)$ process by a factor of 2–3 and for presentation in Fig. 4 the

VM predictions have been multiplied by a factor of 0.4. Despite the overestimation, the VM gives a reasonable description of the shapes of the missing energy spectra for most photon energies and kinematic regions, although the extent of the overestimation depends on both of these variables. However, these variations are small compared with the overall scaling factor which suggests some common error in the calculation of the $pp$ channel for all kinematics. Initial $2\pi$ production processes not at present included in the VM may have a significant contribution for $E_\gamma \geqslant 500$ MeV and would worsen the disagreement.

## V. DIRECT TWO-NUCLEON KNOCKOUT

As already discussed the VM, although giving good indications of the strength of different processes, is not ideally suited to detailed comparisons with the experimental data at low $E_m$ due to the absence of shell structure and the approximate description of nuclear binding. In particular the predicted $2N$ knockout contribution cannot be separated according to emission from specific shell combinations.

The VM calculations presented in the previous section suggest that the strength observed at the lowest missing energies in the $(\gamma,NN)$ reactions is due largely to direct $2N$ knockout. In this section a quantitative check of this assignment is made over the whole measured kinematic range by examining the recoil nucleus momentum distributions as done previously in Refs. [16,17,21]. The recoil momentum distribution shape depends on the shells from which the nucleons are removed and experimentally the $2N$ knockout process from different shell combinations is separated using simple cuts on $E_m$. In $^{12}$C the $E_m \leqslant 40$ MeV region corresponds to absorption on $(1p)^2$ nucleon pairs, while $E_m = 40-70$ MeV corresponds to absorption on $(1s1p)$ pairs [16]. No attempt is made to extract the $(1s)^2$ strength as its contribution is expected to be weak and spread over a wide range of $E_m$.

The Monte Carlo simulations which are used to allow simple models to be compared with the data are outlined in Sec. V A. In Secs. V B and V C the full recoil momentum distributions are studied to assess the relative contribution of direct $2N$ knockout to the cross section in the different $E_m$ regions. Section V D looks in more detail at the high momentum end of the recoil momentum distribution for the knockout of $(1p)^2$ pairs to explore possible SRC effects. In Sec. V E the ratios of strength with $L=0,1,2$ are extracted from the $(1p)^2$ knockout data and compared to the ratios predicted on the basis of the Gottfried model [7] assumptions.

### A. Monte Carlo simulation of the 2*N* knockout process

For comparison with the low $E_m$ data a Monte Carlo model of the direct $2N$ knockout process (MC) is used, the details of which have been described previously [16,17]. The Monte Carlo simulation allows the effect of the detector acceptances to be included in the reaction model predictions. The MC reconstructs the spectra of observables assuming direct $2N$ knockout from a spectating residual nucleus. The Gottfried factorization is implicit in the model with the distribution of initial nucleon pair momenta in the nucleus, $F(P)$, obtained from folding two individual nucleon momentum distributions. The overall missing energy distribution in the residual system after the $2N$ knockout process summed over all break up kinematics is obtained iteratively by adjusting its shape (which is an input to the MC) until the predicted shape of the missing energy distribution visible in the detectors matches that of the experimental data. The iteration procedure is undertaken in region **I** where the contribution from non-$2N$ events is least. By also normalizing the model predictions to the data in this region both the shape and magnitude of distributions in the more extreme kinematic regions (**II** and **III**) can be predicted. This provides a more stringent check of the $2N$ knockout MC model than previously undertaken, allowing comparison of both the shape and angular dependence of the predicted cross sections to the experimental data.

Predictions from a ''phase-space simulation'' (PS) are also presented. In this simulation the available energy in the final state is split between the two nucleons and the recoiling system according to the available phase space. The phase-space prediction gives an indication of the energy available to the recoil nucleus if it is involved in the reaction mechanism as opposed to its spectator role in the $2N$ knockout modelled by the MC. The PS model is normalized to the data separately for each region.

### B. Recoil momentum distributions for $(\gamma,np)$ and the mechanism of the reaction

Recoil momentum distributions from the $^{12}$C$(\gamma,np)$ measurement in the three kinematic regions are shown in Fig. 5 for $E_m \leqslant 40$ MeV.

The shape of the region **I** cross section can be seen to be very well described by the $2N$ knockout MC (thick solid line) for photon energies up to $\sim$600 MeV. The large differences between the $2N$ knockout MC and the PS predictions (dotted line) at higher $E_\gamma$ make the observation even more striking. Although the MC gives slightly poorer detailed agreement with the shape of the $E_\gamma = 600-700$ MeV data the predicted distribution is much closer to the data than that obtained from the PS simulation.

The region **II** and **III** data, away from the back-to-back kinematics, sample larger values of recoil momenta $P_r$ progressively higher with increasing $E_\gamma$. For momenta up to 400 MeV/$c$ both the shape and magnitude of the data are generally well described by the MC model indicating that almost all of the measured yield in these more extreme kinematics can still be attributed to $2N$ knockout. The sensitivity of the cross section in these regions to high pair momenta shows the existence of some additional strength in the experimental data for $P_r \geqslant 400$ MeV/$c$, which is not described by the MC. However, this excess strength is small compared to the main $2N$ knockout strength sampled in region **I**.

Overall these results for $E_m \leqslant 40$ MeV show the dominance of the $2N$ knockout process even when including regions well away from the usual back-to-back kinematics. This reinforces the findings of previous works [16–22] by showing that the observed dominance of $2N$ knockout at low

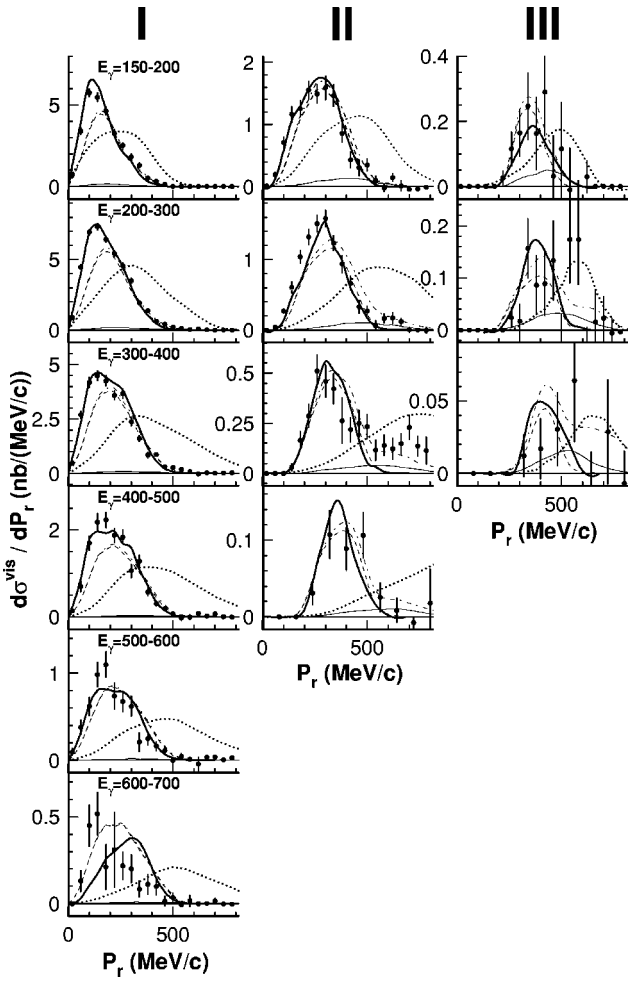


FIG. 5. Recoil momentum distributions for $^{12}C(\gamma,np)$ in the $(1p)^2$ knockout region at $E_m \leq 40$ MeV. The lines on the figure show the predictions of the $2N$ knockout MC (thick solid), phase space model (dotted) and the predicted total (dot-dash), direct $2N$ knockout (dash) and $2N$+FSI (thin solid) cross sections from the Valencia model. The Valencia model predictions have been multiplied by a factor of 0.5.

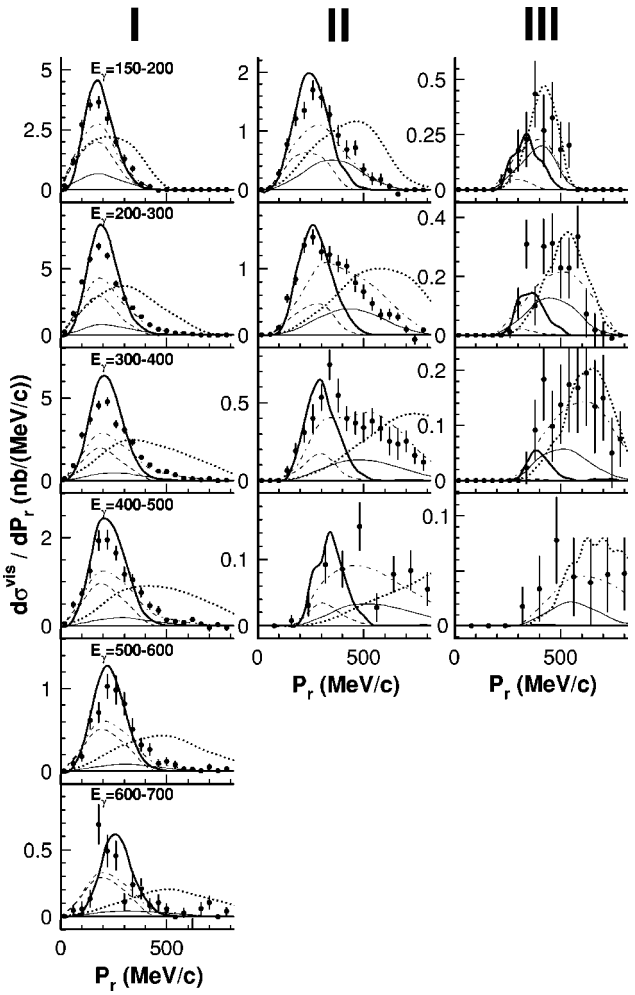


FIG. 6. Recoil momentum distributions for $^{12}C(\gamma,np)$ in the $(1s1p)$ knockout region at $E_m = 40$–$70$ MeV. The different calculations are distinguished as in Fig. 5. The Valencia model predictions have been multiplied by a factor of 0.5.

$E_m$ was not simply due to the positioning of the detectors in a suitable geometry. The data also extend the $E_\gamma$ range and indicate the existence of direct $2N$ knockout of $(1p)^2$ pairs for photon energies well above 400 MeV. Little is known about the reaction mechanism at high photon energy, although the smaller wavelength may produce an increased sensitivity to the shorter range part of the *NN* interaction. The higher $\Delta$ or $N^*$ baryon resonances may also play a role in the knockout mechanism. A detailed study of the $E_\gamma$ dependence of the reaction is presently underway.

The data also indicate that the pair momentum distribution $F(P)$, employed in the MC simulation of the process, accurately represents the momentum distribution of the pair. Since the distribution was derived assuming the *pn* pair is in a relative *S* state it appears that absorption on such pairs is dominant. A more detailed investigation of this assignment is made in Sec. V E.

A further, independent indication of the relative contribution of direct $2N$ knockout is made by comparison of the data in Fig. 5 with the predictions of the Valencia model, although the absence of shell structure in the model and the residual disagreements with the missing energy distributions in Figs. 3 and 4 give expectation of only limited agreement. The VM predictions for the direct $2N$ knockout cross section (dash) and the total $2N$ emission cross section (dot-dash), both multiplied by a factor of 0.5 are plotted. The VM predictions support the previous findings that direct $2N$ knockout dominates the cross section for the removal of $(1p)^2$ nucleons. Despite its limitations the VM gives a consistent description of the variation of the $(\gamma,np)$ cross section at low missing energy and recoil momentum over a wide range of photon energies and kinematics. A more detailed investigation of the high $P_r$ data is presented in Sec. V D.

Data from the $^{12}C(\gamma,np)$ $(1s1p)$ knockout region for $E_m = 40$–$70$ MeV may be more affected by processes other than direct $2N$ knockout as these generally result in more energy being given to the residual system. However as shown in Fig. 6 the $P_r$ dependence of the cross section in region **I** is quite well described up to 700 MeV photon energy by the MC predictions, although the detailed agreement

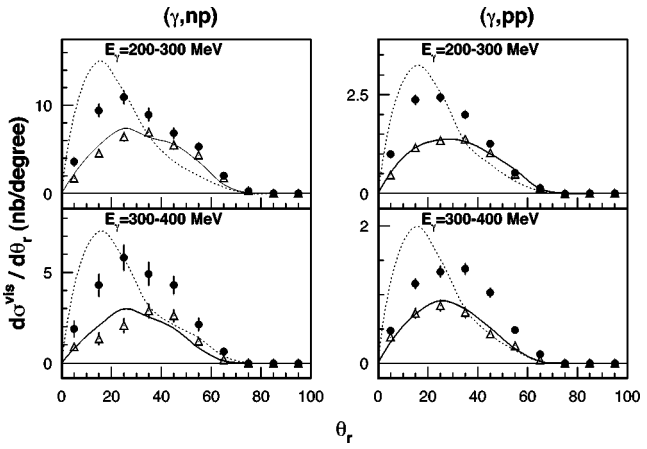


FIG. 7. Angular distribution of the recoil system for $^{12}C(\gamma,np)$ and $(\gamma,pp)$ in the $(1s1p)$ knockout region at $E_m=40-70$ MeV in the region **II** kinematics. The figure shows the distribution for all $P_r$ (circles) and $P_r \leqslant 400$ MeV/$c$ (triangles). The lines on the figure show the predictions of the $2N$ knockout MC (solid) and phase-space model (dotted).

in shape is inferior to that observed for $(1p)^2$ knockout and a small excess strength is evident at high $P_r$. The data in regions **II** and **III** do show significant additional strength at higher $P_r$, the relative contribution of which increases with photon energy. Although unable to describe the strength at high recoil momentum, the MC model does generally reproduce the shape and strength of the lower $P_r$ data, showing that the angular dynamics of the $(1s1p)$ cross section for $P_r \leqslant 300$ MeV/$c$ are consistent with a dominant $2N$ knockout contribution. Indeed, as can be seen in Fig. 7 the distribution in polar angle ($\theta_r$) of the recoil momentum for events in the $E_m=40-70$ MeV region with $P_r \leqslant 400$ MeV/$c$ is consistent with the MC prediction shown by the solid line.

Although the experimental results in region **II** show a significant cross section at high $P_r$ the measured $(1s1p)$ cross section is dominated by the yield in the back-to-back kinematics, which has a distribution close to that expected from direct $2N$ knockout.

The VM predictions shown in Fig. 6 are multiplied by the same factor of 0.5 applied in the $(1p)^2$ region. The largest contribution in the back-to-back kinematics of region **I** is predicted to be from direct $2N$ knockout but a significant contribution from other processes is also suggested and this could explain the lack of detailed agreement between the MC and experiment in Fig. 6 and Refs. [16,21]. The predicted relative contribution of the other processes increases rapidly away from the back-to-back kinematics.

### C. Recoil momentum distributions for $(\gamma,pp)$ and the mechanism of the reaction

The cross section for the $(\gamma,pp)$ reaction at low $E_m$ is reduced, as noted above, at high $E_\gamma$ due to the restricted upper energy limit of TOF for identifying protons. Recoil momentum distributions are therefore only presented for $E_\gamma \leqslant 600$ MeV in Figs. 8 and 9.

For $E_m \leqslant 40$ MeV shown in Fig. 8 the MC describes the shape of the available region **I** data reasonably well, although the detailed agreement is not as good as that observed for the $(\gamma,np)$ reaction. The model predicts strength at low $P_r$ which is not visible in the experimental data, a small but consistent effect also evident in earlier comparisons [16,21] under different kinematic conditions. In Refs. [16,21] this disagreement was interpreted as a sign of contributions from mechanisms other than direct $pp$ knockout, but it is now thought to be the result of an inappropriate pair momentum distribution $F(P)$ in the MC simulation. This is discussed in Sec. V E. For regions **II** and **III** the MC model again gives a reasonable general description of the large changes in strength and shape of the lower $P_r$ data but as already observed in the corresponding $(\gamma,np)$ distributions it does not account for strength at $P_r \geqslant 500$ MeV/$c$. However when all three kinematic regions are considered direct knockout can be seen to account for most of the measured strength.

The VM predictions shown in Fig. 8 have been multiplied by a factor of 0.15 for comparison with the experimental data. The direct $2N$ knockout process is predicted to dominate the low $P_r$ yield in all kinematic regions, giving support to the above interpretation. The VM also gives a qualitative description of the relatively small strength at high $P_r$, attributing most of the yield to processes other than direct knockout.

Figure 9 shows the $^{12}C(\gamma,pp)$ recoil momentum distributions for $E_m=40-70$ MeV. In the back-to-back kinematics of region **I** the MC predictions of direct knockout of $(1s1p)$ pairs (thick solid line) do not describe the data for $P_r$ above $\sim 300$ MeV/$c$ indicating a large contribution from other processes. This is also evident in the data from Refs. [16,21]. The trend is accentuated in regions **II** and **III**. The MC gives a reasonable general description of the low $P_r$ cross section as shown by the $\theta_r$ distributions plotted in Fig. 7 but cannot describe the significant strength in the data at higher $P_r$.

The VM predictions multiplied by a factor of 0.15 are also compared with the experimental data in Fig. 9. The VM does not predict that direct $2N$ knockout is dominant at any photon energy, even for region **I**. This result brings into question the validity of the normalization of the $2N$ knockout MC to the experimental data in this region. For the other kinematic regions direct knockout is predicted to play an even smaller role with the bulk of the measured cross section attributed to other processes by the VM which does reproduce the general trends of the recoil momentum distributions. A study of direct knockout of $(1s1p)$ proton pairs will only be possible if an accurate treatment of the contribution of other processes is available.

### D. Recoil momentum distribution at high $P_r$— Possible short-range effects

It has often been suggested that a study of the $(\gamma,NN)$ reaction can produce information on SRC's since the correlations can directly affect the absorption mechanism. However, it is possible that this information can be obtained from the $(\gamma,NN)$ data in a different way, less sensitive to the details of the reaction mechanism, which are still not fully understood. In Ref. [8] Orlandini and Sarra calculate the effect of SRC's on the pair momentum distribution in $^{16}O$.

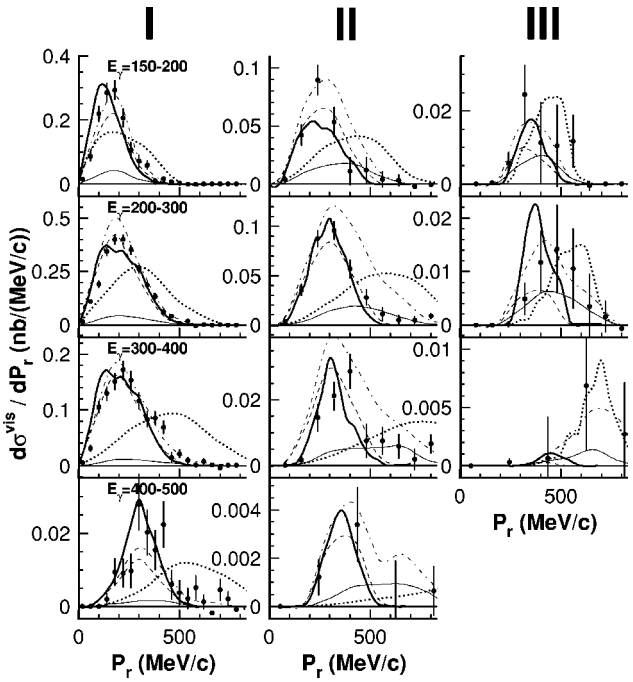


FIG. 8. Recoil momentum distributions for $^{12}$C($\gamma$,$pp$) in the $(1p)^2$ knockout region at $E_m \leq 40$ MeV. The different calculations are distinguished as in Fig. 5. The Valencia model predictions have been multiplied by a factor of 0.15.

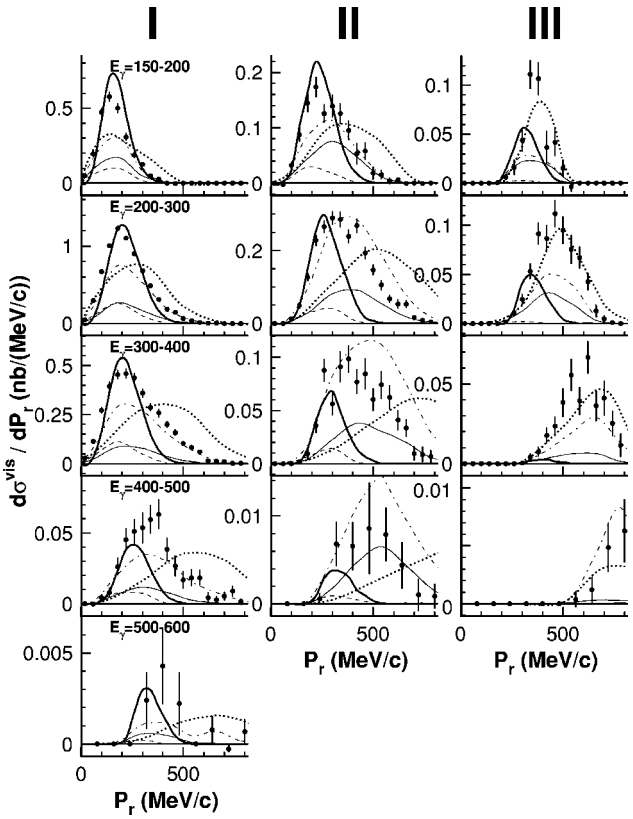


FIG. 9. Recoil momentum distributions for $^{12}$C($\gamma$,$pp$) in the $(1s1p)$ knockout region at $E_m = 40-70$ MeV. The different calculations are distinguished as in Fig. 5. The Valencia model predictions have been multiplied by a factor of 0.15.

Each of the nucleons, which make up the pair, carries information on its previous short-range collisions in the form of an enhancement of its momentum wave function at high momentum and this produces enhancements in the momentum distribution of the pair above $\sim 450$ MeV/$c$. In the present results SRC's would show up as an excess strength at high recoil momentum $P_r$ compared to the $2N$ knockout Monte Carlo prediction which does not take account of correlations. It is apparent in Figs. 5 and 8 that such an excess strength is observed even for the lowest missing energy bin, $E_m \leq 40$ MeV, where final-state interactions and other mechanisms are least important. Recent $^{12}$C($e$,$e'pp$) data [39] also shows significant excess strength in this high momentum region.

A search for SRC effects has been carried out using the present $E_m \leq 40$ MeV data for the ($\gamma$,$np$) reaction since, as discussed in Secs. V B and V E, the form of the pair momentum distribution is better established for *np* emission than for ($\gamma$,$pp$). The ratio of the experimental data to the MC model predictions is presented in Fig. 10 to highlight the excess at high $P_r$. Although there is some scatter in the points Fig. 10 does indeed show an excess of measured strength compared to the MC calculation for $P_r \geq 450$ MeV/$c$ and the $P_r$ dependence of the ratio is similar for all kinematic regions and photon energies. The calculation of Orlandini and Sarra [8] (solid line) is in reasonable agreement with the experimental data. It shows the ratio of the pair momentum distribution which they obtain for $^{16}$O including SRC's divided by the distribution obtained without SRC's. The agreement with the data should be treated with caution since the calculation includes all excitations in the residual nucleus, whereas the present results include only low-lying states. Equivalent calculations for one-nucleon knockout find that the additional high momentum strength produced by SRC's is predominantly associated with large excitations in the residual nucleus.

Two other possible sources of the excess yield have also been examined. First, the effect which would be obtained by replacing the harmonic-oscillator (HO) wave functions used in the MC model with more realistic nucleon wave functions was investigated. The dashed (dotted) lines show the ratio of the pair momentum distribution obtained with Woods-Saxon (Hartree-Fock) wave functions [40] to the HO result. These indicate that the excess is not a result of an inadequacy peculiar to the HO wave functions. Second the VM predictions (Fig. 5) were examined in more detail to see if processes other than direct $2N$ knockout could be responsible for the measured excess. The result is inconclusive; other processes do produce an excess above $P_r \sim 450$ MeV/$c$ but with only about 50% of the observed strength. Furthermore, since a large part of the strength is due to $2N$ knockout followed by FSI, it is important to know how significantly the FSI changes $P_r$ in order to know whether such $2N$+FSI events should be counted as part of the excess or part of the basic $2N$ strength, and this information is not at present available from the VM code. Although Fig. 10 suggests a measurable influence of SRC's on the pair momentum distribution, more

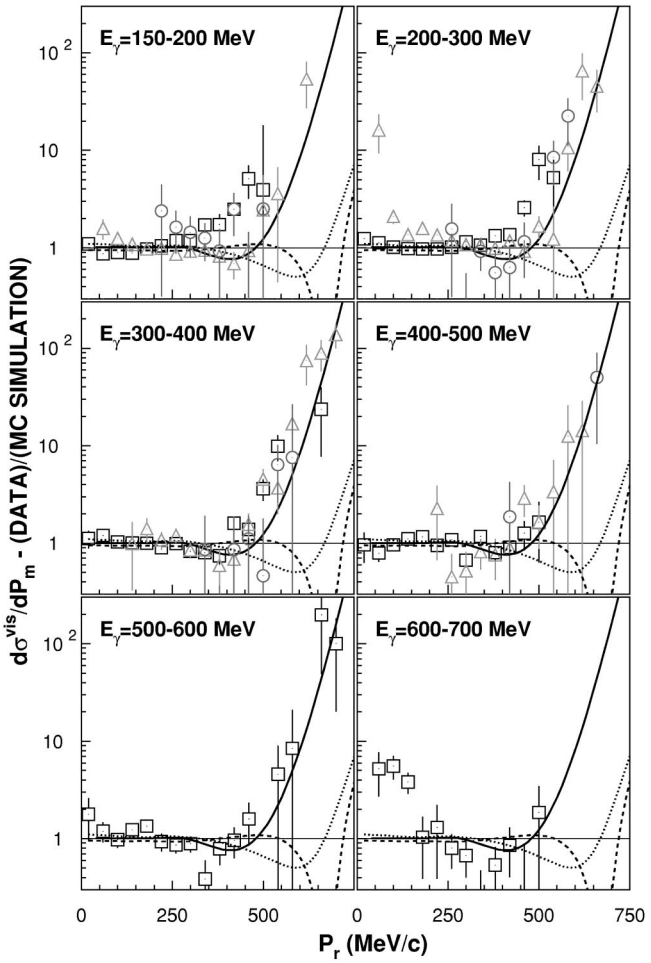


FIG. 10. Recoil momentum distributions for $^{12}$C$(\gamma,np)$ for $E_m \leqslant 40$ MeV presented as a ratio to the $2N$ knockout MC predictions. The plot shows data from the kinematic regions I (squares), II (triangles), and III (circles) described in the text. The solid line shows the ratio of the pair momentum distribution obtained with SRC's to that calculated without SRC's for $^{16}$O [8]. The dotted (dashed) lines show the ratio of the $P_r$ distribution predicted using Hartree-Fock (Woods-Saxon) wave functions (with no SRC's) to that using HO.

detailed analysis of other contributing mechanisms is needed.

### E. The angular momentum components of $F(P)$ and the limitations of the Gottfried approach

In Secs. V B and V C the $(\gamma,NN)$ recoil momentum distributions are compared with simulations which use the Gottfried expression for $F(P)$. For the $(\gamma,pp)$ case these comparisons show the same small, systematic discrepancies seen in earlier experiments [16,21]. It is explained below that these discrepancies are an expected consequence of the limitations of the Gottfried approach. In fact a detailed examination of the recoil momentum spectra can be used to explore the expected sensitivity of $2N$ knockout to the nature of the residual state and hence to the reaction mechanism. Below this is done for the $(1p)^2$ knockout region since this feeds the relatively well separated lower lying bound states.

In the $(\gamma,NN)$ reaction the spin and parity of the final states in the nucleus can act as a filter with particular states populated only by photoabsorption on pairs in specific combinations of relative $(l)$ and c.m. $(L)$ angular momentum states. For $(1p)^2$ knockout $L=0,1,2$ are allowed for the initial pair and the present data are, therefore, fitted with this combination $\Sigma_L a_L F_L(P)$ where the pair-momentum distributions, $F_L(P)$, for each angular momentum value are calculated from harmonic-oscillator wave functions. To conserve spin and parity in the knockout of $(1p)^2$ pairs even (odd) valued $l$ states must couple to even (odd) valued $L$ states. The allowed combinations for each state in the residual nucleus are tabulated in [10,13]. The Gottfried zero-range approximation, which implies that the initial pair is in a relative $S$ state, leads to a pair momentum distribution for an $np$ pair having $L$ components in the ratio 0.33:0:0.67 for $L=0,1,2$, respectively. Using more realistic $^{12}$C wave functions [41] this becomes 0.40:0:0.60 for pairs in spin triplet $(S=1)$ states, which are thought to make the main contribution to the $(\gamma,np)$ reaction [7]. Before being fitted the recoil momentum distributions have been corrected for the effect of detector acceptance using a correction function determined at each photon energy from the $2N$ knockout MC simulation. To improve the presentation of the fits in Figs. 11 and 12, the $\mathbf{P}^2$ phase-space factor in the momentum distributions has been divided out.

Fits to the $(\gamma,np)$ recoil momentum distributions are presented in Fig. 11 for two photon energy bins and two 6 MeV wide bins of observed excitation energy, $E_X$, in the residual $^{10}$B nucleus, $-3 \leqslant E_X \leqslant 3$ MeV and $3 \leqslant E_X \leqslant 9$ MeV. The data for $P_r \leqslant 400$ MeV/$c$ are fitted with combinations of $L=0,1,2$ distributions and the relative contributions extracted from the fit are shown in Table I. The $^{10}$B nucleus has many levels in each of the fitted $E_X$ regions. Nonetheless differences are already evident between the two excitation regions, although the separation of transitions to different individual states will have to wait for a measurement with finer resolution, as already proposed at Mainz [42].

The $P_r$ distribution of the $E_X \leqslant 3$ MeV data is well described in both $E_\gamma$ regions by $L=0,2$ contributions alone, with a relative contribution close to that expected from the knockout of pairs initially in relative $S$ states. However, the higher $E_X$ region does indicate a significant $L=1$ contribution, which is largest at low $E_\gamma$. For direct $2N$ knockout this suggests the contribution of pairs in relative $P$ states. Although FSI effects could possibly add strength in this $L=1$ region, the predictions of the Valencia model indicate little contribution from processes other than direct $2N$ knockout. The microscopic theory by Ryckebusch [11], which does not make any restrictions on the relative wave function of the initial nucleon pair, does in fact predict a contribution from relative $P$ states at photon energies below $\sim$200 MeV where the larger magnitude of the photon wavelength would lead one to expect a breakdown in Gottfried's ''zero-range'' approximation. On average this contribution increases the calculated cross section in the 150–200 MeV region for $^{16}$O by $\sim$15% which is comparable with the $L=1$ strength averaged over both $E_X$ bins in Fig. 11. The relative $P$-wave contribu-

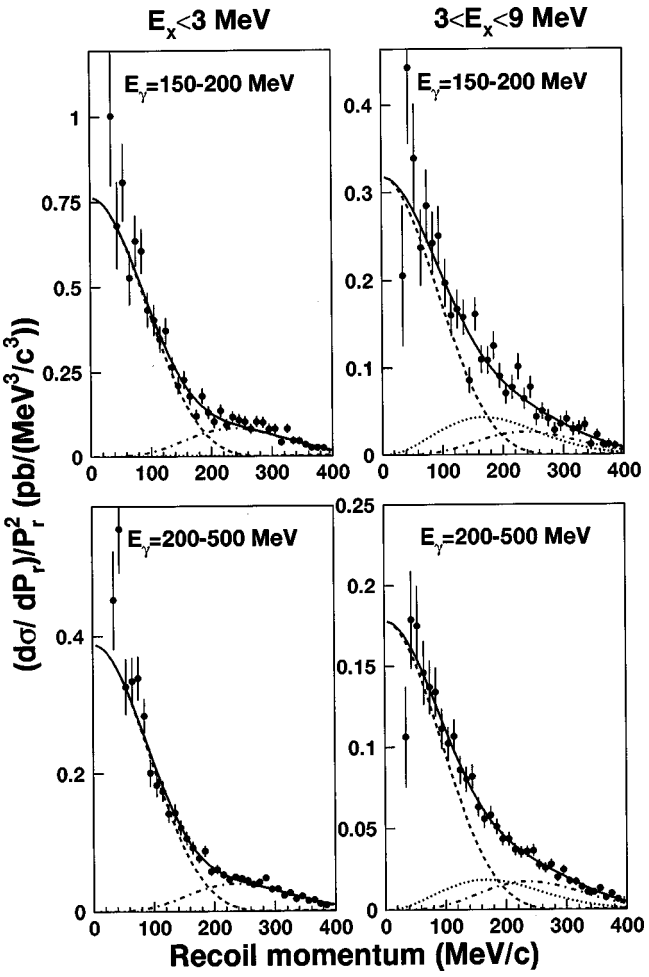


FIG. 11. $^{12}$C($\gamma$,$np$) $P_r$ distributions for two $E_m$ cuts within the $(1p)^2$ knockout region. The data have been corrected for phase-space and detector effects. The curves show the result of fitting the data with the combination $\Sigma_L a_L F_L(P)$ (solid) and the separate contributions from the $L=0$ (dash), $L=1$ (dotted), and $L=2$ (dot-dash) components. The relative contribution of the different components are shown in Table I.

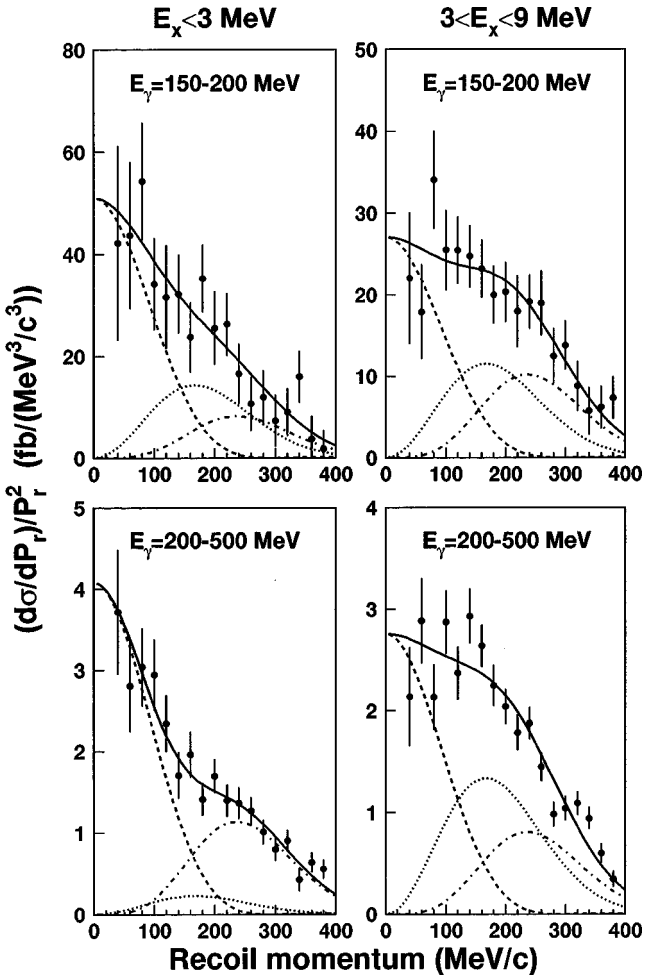


FIG. 12. $^{12}$C($\gamma$,$pp$) $P_r$ distributions for two $E_m$ cuts within the $(1p)^2$ knockout region. Labeling as in Fig. 11.

tion is predicted to decrease with increasing $E_\gamma$, as observed in the data.

For proton-proton knockout the residual $^{10}$Be nucleus has a larger spacing between the lowest lying residual states $[0^+(\text{g.s}),2^+(3.37\ \text{MeV})]$ than $^{10}$B so the $E_X \leqslant 3$ MeV cut will emphasize the cross section to the $0^+$ ground state, although the experimental resolution does not permit a total separation. For ($\gamma$,$pp$) the $\Delta N \rightarrow NN$ knockout mechanism following initial $\Delta$ excitation is suppressed for magnetic dipole ($M1$) photoabsorption on $^1S_0$ proton-proton pairs because of total angular momentum and parity conservation requirements in the decay of the intermediate $N$-$\Delta$ state [15]. The $\Delta$ mechanism only contributes to $2N$ knockout through photon absorption on pairs in higher relative waves than the $S$ state or transitions involving higher multipolarity.

Fits to the ($\gamma$,$pp$) recoil momentum spectra are presented in Fig. 12 and the relative contributions for different $L$ values are shown in Table I. The $E_X \leqslant 3$ MeV data shows the knockout of proton-proton pairs with $L=1$ is far more probable than that observed for the ($\gamma$,$np$) reaction, suggesting $^3P$ pairs give a significant contribution to the $pp$ knockout process. The $L=0,2$ components in the momentum distribution indicate that $^1S_0$ knockout contributes to the cross section ($^1D_2$ knockout is predicted to give small contributions in this $E_\gamma$ region [10]), mainly through $L=2$ pairs and increases in importance with $E_\gamma$. The increase of $^1S_0$ knockout with photon energy could be due to either a larger SRC contribution or a significant contribution from higher multipolarity photons to the knockout process via the $\Delta$ mechanism.

In going from lower excitation to the $3 \leqslant E_X \leqslant 9$ MeV region, the relative contribution of $L=0$ knockout in both $E_\gamma$ regions is reduced, indicating that this process mainly feeds the lower lying bound states in the residual nucleus. $L=1$ knockout gives a large contribution to the cross section in both photon energy regions feeding the $1^+$ and possibly also $2^+$ state in this region [10,13]. $^1S_0$ knockout with $L=2$ gives a similarly large contribution in this $E_X$ region.

The results presented above reveal the limitations of the Gottfried approach to ($\gamma$,$NN$) reactions, in which only nucleon pairs in relative $S$ states contribute. For the ($\gamma$,$pp$) reaction the present analysis reveals a large contribution from $^3P$ pairs. This explains the lack of detailed agreement

TABLE I. Ratio $a_0:a_1:a_2$ obtained from fitting the $^{12}C(\gamma,np)$ and $^{12}C(\gamma,pp)$ recoil momentum spectra with the combination $\Sigma_L a_L F_L(P)$ for two excitation regions of the residual nucleus and $E_\gamma$ regions below and through the $\Delta$ resonance. Errors in the fitted parameters are shown in brackets.

| | $E_\gamma$ | $E_X \leqslant 3$ MeV | $3 \leqslant E_X \leqslant 9$ MeV |
|---|---|---|---|
| $(\gamma,np)$ | 150–200 | 0.35(±0.02): 0.02(±0.13): 0.63(±0.07) | 0.20(±0.01): 0.53(±0.13): 0.27(±0.07) |
| | 200–500 | 0.37(±0.01): 0.01(±0.10): 0.62(±0.05) | 0.22(±0.01): 0.43(±0.08): 0.35(±0.04) |
| $(\gamma,pp)$ | 150–200 | 0.11(±0.02): 0.59(±0.29): 0.30(±0.18) | 0.06(±0.01): 0.54(±0.17): 0.40(±0.12) |
| | 200–500 | 0.15(±0.02): 0.16(±0.17): 0.69(±0.09) | 0.06(±0.01): 0.62(±0.09): 0.32(±0.05) |

seen in Fig. 8 and in Refs. [16,21] between $(\gamma,pp)$ data and a $2N$ knockout MC model based on the Gottfried approach. The magnitude of the asymmetry from recent $(\vec{\gamma},pp)$ measurements for $^{12}C$ [24] and $^{16}O$ [25] is also inconsistent with that predicted for solely $^1S_0$ knockout.

Although the knockout of $^3P$ pairs via the $\Delta$ mechanism gives a large contribution to the $(\gamma,pp)$ cross section, $^1S_0$ knockout, which may be sensitive to SRC's, is also significant especially in the lowest $E_X$ region. A large $^1S_0$ cross section at low excitation has also been inferred from recent $^{16}O(e,e'pp)$ data [43–45] in which the cross section for $^1S_0$ knockout to the ground and low-lying states was predicted to be dominantly due to mechanisms involving SRC's. However real photon experiments are expected to show less sensitivity to SRC's and recent angular distribution measurements for $^{12}C(\gamma,pp)$ at $E_\gamma = 250$–$300$ MeV [23] are consistent with $\Delta$ excitation via higher photon multipoles. The possibility that sensitivity to SRC's can be regained in a higher resolution $(\gamma,pp)$ measurement in a specific kinematic region is presently being investigated.

## VI. CONCLUSIONS

The $^{12}C(\gamma,NN)$ reactions have been measured for a wide kinematic range including regions away from the back-to-back geometry of most previous experiments. The general features of the $^{12}C(\gamma,np)$ reaction are well described for all $E_m$ by the Valencia model, even in regions away from the back-to-back kinematics. This gives much improved confidence that the processes included in the model can give a good general description of the reaction. The VM overestimates the corresponding $^{12}C(\gamma,pp)$ cross section by a factor of $\sim 3$ which is photon energy dependent and also to a lesser extent angle dependent. This large overestimation of the cross section is similar in all of the kinematic regions studied. For both channels the $2N$ knockout process, with little distortion from FSI or non-$2N$ processes, is predicted to give the largest contribution at low missing energy.

A detailed study of the direct $2N$ knockout process was carried out for the low $E_m$ data. For excitation regions of the residual nucleus which can be populated by $(1p)^2$ knockout the shape of the $(\gamma,np)$ recoil momentum distributions could be well described by a $2N$ knockout Monte Carlo (MC) model, which predicted the pair momentum from harmonic-oscillator wave functions. For $(\gamma,pp)$ the agreement was slightly poorer. The large changes in the shape and magnitude of the cross section away from the back-to-back kinematics are in good general agreement with the MC predictions, which were normalized to the data in the back-to-back kinematics, indicating for the first time that the angular dynamics of the $2N$ knockout process is well described by this simple model.

The sensitivity of the $2N$ knockout reaction to the nature of the residual nuclear state was explored by separating two excitation regions of the residual nucleus, $E_X \leqslant 3$ MeV and $3 \leqslant E_X \leqslant 9$ MeV. The shape of the cross section as a function of recoil momentum was studied by fitting the distribution with contributions from $L=0,1,2$ pairs. For $(\gamma,np)$ most of the data could be well fitted by $L=0$ and 2 distributions only, and the ratio of the two contributions was in reasonable agreement with the Gottfried prediction. For $(\gamma,pp)$ the recoil momentum data indicated a significant contribution from pairs with $L=1$, the relative contribution of which was larger for the higher excitation region. The $L=1$ component was attributed to the knockout of $^3P$ pairs and indicated a significant breakdown of the Gottfried assumptions for this channel. The data did, however, indicate significant $^1S_0$ knockout, the relative contribution of which was larger for low excitation and increased with $E_\gamma$.

At large recoil momenta the $(1p)^2$ data indicate a small yield in excess of that which can be explained by the simple $2N$ knockout model. The excess showed little dependence on kinematics or photon energy and was quite well described by the calculated effects of short range correlations on a pair momentum distribution for $^{16}O$. However, predictions from the Valencia model suggest caution before interpreting the small cross section at high recoil momentum as being entirely due to the effect of correlations since a significant fraction of the strength is predicted to arise from non-$2N$ processes.

For the $E_m = 40$–$70$ MeV region, where $(1s1p)$ knockout is expected to contribute, the detailed agreement of the shape of the recoil momentum distributions with the MC model was inferior to that observed for $(1p)^2$ and a significant yield at high recoil momenta was present. For the back-to-back kinematics the Valencia model indicated a large $2N$ knockout component but away from these kinematics non-$2N$ processes generally dominate the cross section.

## ACKNOWLEDGMENTS

This work was supported by the U.K. EPSRC, the British Council, the DFG (Mu 705/3), BMFT (06 Tü 656), DAAD (313-ARC-VI-92/118), the EC [SCI.0910.C(JR)], and NATO (CRG 920171, CRG 970268). T.T-H.Y, S.M, J.A.M, and D.P.W would like to thank the EPSRC for financial support during this work.

[1] J. M. Laget, Nucl. Phys. **A497**, 391 (1989); J. Phys. G **14**, 1445 (1988).
[2] R. C. Carrasco and E. Oset, Nucl. Phys. **A536**, 445 (1992); R. C. Carrasco, E. Oset, and L. L. Salcedo, *ibid.* **A541**, 585 (1992); R. C. Carrasco, M. J. Vicente-Vacas, and E. Oset, *ibid.* **A570**, 701 (1994).
[3] T. Lamparter *et al.*, Z. Phys. A **355**, 1 (1996).
[4] P. D. Harty *et al.*, Phys. Rev. C **57**, 123 (1998).
[5] G. E. Cross *et al.*, Nucl. Phys. **A593**, 463 (1995).
[6] E. D. Hackett *et al.*, Phys. Rev. C **53**, R1047 (1996).
[7] K. Gottfried, Nucl. Phys. **5**, 557 (1958).
[8] G. Orlandini and L. Sarra, in Proceedings of the Second Workshop On Electromagnetically Induced Two-Nucleon Emission, Gent, 1995, edited by J. Ryckebusch and M. Waroquier, p. 1.
[9] C. Giusti, F. D. Pacati, and M. Radici, Nucl. Phys. **A546**, 607 (1992); C. Giusti and F. D. Pacati, *ibid.* **A535**, 573 (1991); **A571**, 694 (1994); **A585**, 618 (1995); S. Boffi, C. Giusti, F. D. Pacati, and M. Radici, *ibid.* **A564**, 473 (1993).
[10] C. Giusti and F. D. Pacati, Nucl. Phys. **A641**, 297 (1998).
[11] J. Ryckebusch, M. Vanderhaeghen, L. Machenil, and M. Waroquier, Phys. Lett. B **291**, 213 (1992).
[12] J. Ryckebusch, M. Vanderhaeghen, L. Machenil, and M. Waroquier, Phys. Lett. B **316**, 17 (1992); J. Ryckebusch, M. Vanderhaeghen, L. Machenil, V. Van der Sluys, and M. Waroquier, Phys. Rev. C **49**, 2704 (1994); J. Ryckebusch, M. Vanderhaeghen, L. Machenil, and M. Waroquier, Nucl. Phys. **A568**, 828 (1994); J. Ryckebusch, M. Vanderhaeghen, L. Machenil, and M. Waroquier, *ibid.* **A580**, 551 (1994).
[13] J. Ryckebusch, D. Debruyne, and W. V. Nespen, Phys. Rev. C **57**, 1319 (1998).
[14] J. Ryckebusch, Phys. Lett. B **383**, 1 (1996).
[15] P. Wilhelm, J.A. Niskanen, and H. Arenhovel, Phys. Rev. C **51**, 2841 (1995).
[16] J. C. McGeorge *et al.*, Phys. Rev. C **51**, 1967 (1995).
[17] I. J. D. MacGregor *et al.*, Nucl. Phys. **A533**, 269 (1991).
[18] S. N. Dancer *et al.*, Phys. Rev. Lett. **61**, 1170 (1988).
[19] S. M. Doran *et al.*, Nucl. Phys. **A559**, 347 (1993).
[20] S. Klein, Ph.D. thesis, University of Tübingen, 1990.
[21] P. D. Harty *et al.*, Phys. Lett. B **380**, 247 (1996).
[22] P. Grabmayr *et al.*, Phys. Lett. B **370**, 17 (1996).
[23] T. T-H. Yau, Ph.D. thesis, University of Glasgow, 1996; T. T-H. Yau *et al.*, Eur. Phys. J. A **1**, 241 (1998); I. J. D. MacGregor *et al.*, Phys. Rev. Lett. **80**, 245 (1998).
[24] C. J. Y. Powrie *et al.* (unpublished); I.J.D. MacGregor, in Proceedings of the Fourth Workshop on Electromagnetically Induced Two Hadron Emission, Granada, 1999, edited by C. Garcia-Recio, P. Grabmayr, A. M. Lallena, and R. O. Owens, p. 339.
[25] R. Lindgren *et al.*, Brookhaven National Laboratory Report No. 65187, 1998.
[26] S. Franczuk *et al.*, Phys. Lett. B **450**, 332 (1999).
[27] H. Herminghaus, Proc. of the Linear Accelerator Conference, Albuquerque, NM, 1990; T. Walcher, Prog. Part. Nucl. Phys. **24**, 189 (1990).
[28] I. Anthony, J. D. Kellie, S. J. Hall, G. J. Miller, and J. Ahrens, Nucl. Instrum. Methods Phys. Res. A **301**, 230 (1991); S. J. Hall, G. J. Miller, R. Beck, and P. Jennewein, *ibid.* **368**, 698 (1996).
[29] I. J. D. MacGregor *et al.*, Nucl. Instrum. Methods Phys. Res. A **382**, 479 (1996).
[30] P. Grabmayr *et al.*, Nucl. Instrum. Methods Phys. Res. A **402**, 85 (1998).
[31] CERN Computer Newsletter 200, 13 (1990).
[32] T. Lamparter, Ph.D. thesis, University of Tübingen, 1997.
[33] R. A. Cecil, B. D. Anderson, and R. Madey, Nucl. Instrum. Methods **161**, 439 (1979).
[34] J. C. McGeorge (private communication); D. P. Watts, Ph.D. thesis, University of Glasgow, 1997.
[35] D. A. Jenkins, P. T. Debevec, and P. D. Harty, Phys. Rev. C **50**, 74 (1994).
[36] P. Rossi *et al.*, Phys. Rev. C **40**, 2412 (1989).
[37] A. Braghieri *et al.*, Phys. Lett. B **363**, 46 (1995).
[38] J. A. Gómez Tejedor, M.J. Vicente-Vacas, and E. Oset, Nucl. Phys. **A588**, 819 (1995).
[39] K. I. Blomqvist *et al.*, Phys. Lett. B **421**, 71 (1998).
[40] J. Ryckebush (private communication).
[41] A. Mondry, Ph.D. thesis, University of Tübingen, 1997.
[42] P. Grabmayr *et al.*, MAMI proposal Nr: A2/4-97.
[43] C. J. G. Onderwater *et al.*, Phys. Rev. Lett. **78**, 4893 (1997).
[44] C. J. G. Onderwater *et al.*, Phys. Rev. Lett. **81**, 2213 (1998).
[45] G. Rosner, Prog. Part. Nucl. Phys. **44**, 99 (2000).